

The Influence of Mild Steel Metallurgy on the Initiation of Localized CO₂ Corrosion in Flowing Conditions

Emad Akeer, Bruce Brown, Srdjan Nestic

Institute for Corrosion and Multiphase Technology
Department of Chemical and Biomolecular Engineering
Ohio University
342 W. State St.
Athens, OH 45701

ABSTRACT

The environmental conditions encountered in oil and gas wells can cause severe corrosion to mild steel tubing and pipelines and the microstructure and chemical composition of steel are considered to be important variables that affect the resistance of steel to corrosion.

Five different pipeline steels with different chemical composition and microstructure were chosen to investigate the effect of their metallurgy on the properties of iron carbonate and related corrosion phenomena that could lead to localized corrosion. The effect of a high liquid flow rate on a pre-formed iron carbonate corrosion product layer was studied at 80°C, pH 6.6, and 1.5 pCO₂. Iron carbonate layer, initially pre-formed on each steel at relatively low wall shear stress (35 Pa), was then exposed to high wall shear stress (535 Pa) for 3 days. For all tested steels, the pre-formed iron carbonate layer reduced the general corrosion rate to less than 0.5 mm/y after 2 days, but the increase in wall shear stress caused partial loss of the protective iron carbonate layer. All steels suffered localized or pitting corrosion, but the penetration rates of pitting found in normalized steels was much lower than that of quenched and tempered steels.

Keywords: CO₂ corrosion, wall shear stress, iron carbonate, steel microstructure, normalized, quenched and tempered.

INTRODUCTION

The environmental conditions encountered in oil and gas wells can cause severe corrosion to mild steel tubing and pipelines. Despite this limitation, mild steel is still preferred because it is considered the most cost effective option compared with more expensive alternative materials such as stainless steels (SS), even when including the cost of corrosion inhibition. The ability to protect mild steel pipelines from corrosion is affected by the water chemistry, fluid velocity, CO₂ content, and temperature; however, the microstructure and chemical composition of steel are also considered to be important variables¹⁻⁶ that affect the resistance of steel to corrosion.

The use of mild steel in oil and gas pipelines depends on either formation of protective corrosion product layers or use of corrosion inhibitors^{5,6}. However, performance of protective corrosion products and corrosion inhibitor are influenced by chemical composition and microstructure of steel¹⁻⁴. Although there are no significant effects of alloying elements and microstructure on corrosion rate in environments where protective layers do not form, when they do, the microstructure and is suspected to cause local areas of accelerated corrosion which vary with metallurgical characteristics.

Localized corrosion takes place when small areas of a metal surface selectively experience a higher corrosion rate compared to the rest of the surface. Localized corrosion is known to be very dangerous as it can cause short term failure, over a period of months, of pipelines designed to last for over 20 years. The development of a protective layers on the mild steel surfaces is desirable to limit the corrosion rate, but this layer is highly dependent on surface features and material characteristics. Breakdown of protective layers that form on the mild steel can lead to localized corrosion. Two mechanisms that can cause damage of protective layers are chemical attack and mechanical breakdown. If a large area of a mild steel surface is covered by a protective layer, then failure of a small area on that surface is expected to lead to development of a galvanic cell and accelerate corrosion by an electrochemical mechanism. The chemical and mechanical effect on localized corrosion are dependent on water chemistry and flow parameters; however, it is suspected that chemical composition and microstructure of steel can play a major role in localized corrosion mechanisms in CO₂ corrosion.

Many studies have discussed the influence of chemical composition and microstructure of carbon and low alloy steels in CO₂ corrosion¹⁻⁶; however, most of these studies did not give a clear explanation relating microstructure and chemical composition of steel to localized corrosion mechanisms in CO₂ corrosion.

The goal of this work is to shed light on the influence of pipeline materials on CO₂ corrosion of mild steel, with a focus on mechanisms that lead to localized corrosion.

EXPERIMENTAL PROCEDURE

Materials

Metallographic analysis

The steels in the test study are X52, X65I, X65II, X70, and A106GRB. The steels were machined from different pipeline steel spools. The steels were chosen in order to obtain different microstructural and compositional characteristics. The steels were submitted to Laboratory Testing Inc[†] for chemical composition evaluation and three of them (X65I, X65II, X70) were found to be in conformance to UNS G15130, A106GRB was in conformance to UNS G10290, and X52 was in conformance to UNS G15250. The Unified Numbering System (UNS) of Ferrous Metals and Alloys UNS16 determine the requirements of American Iron and Steel Institute (AISI) and Society of Automobile Engineers (SAE) carbon and alloy steels, as shown in Table 1.

Microstructure

Three sections from different planes were cut from each steel and mounted in Bakelite[‡] for metallographic analysis using the polishing and etching procedure. Micrograph images of all steels had been taken using Alicona Infinite Focus Microscope (IFM) to examine the microstructure of each steel.

Table 1
Chemical Composition of X65I, X65II, and X70 Steels

Element	(UNS G15130)		(UNS G15250)		(UNS G10290)
	X65I/%	X70/%	X65II/%	X52/%	A106GRB/%
Al	0.037	0.033	0.024	0.056	0.031
C	0.14	0.071	0.07	0.26	0.27
Cr	0.14	0.23	0.052	0.037	0.069
Cu	0.12	0.018	0.27	0.006	0.089
Mn	1.18	1.38	1.31	1.01	0.82
Mo	0.14	0.094	0.026	0.004	0.003
Ni	0.38	0.092	0.10	0.024	0.049
P	0.010	0.011	0.008	0.010	0.014
S	0.004	0.004	0.006	0.012	0.003
Si	0.24	0.13	0.27	0.023	0.27
Ti	0.005	0.007	0.016	0.002	0.002
V	0.056	0.05	0.025	0.063	0.003

Corrosion Experiments

The corrosion experiments were conducted in the Thin Channel Flow Cell (TCFC) which was developed at the Institute for Corrosion and Multiphase Technology-Ohio University⁸ as shown in Figure 1. The TCFC provides realistic flow conditions with easier operation compared to large scale systems and is designed for high wall shear stress flow and corrosion testing.

Wall shear stress Determination

The wall shear stress of the TCFC was determined at 25°C using three different methods:

[†] Laboratory Testing Inc. 2331 Topaz Drive, Hatfield, PA 19440 "UNS NUMBER INDEX", http://www.astm.org/DIGITAL_LIBRARY/MNL/SOURCE_PAGES/MNL12062D_index.pdf. Sep. 2007.

[‡] Trade name for plastic mounting material. Bakelite is a synthetic resin chemically formulated. The Bakelite powder is used with specimens mounting press machine for mounting of specimens.

- The wall shear stress sensor acquired from the Lenterra Company[§].
- By measurement of the pressure drop between two points, as shown in Figure 1, followed by calculation of wall shear stress using equation (1):

$$\tau = \frac{(p_1 - p_2) * 100000 * h * w}{(2 * (h + w) * l)} \quad (1)$$

- Calculation of the friction factor using Dean's formula⁹, Equation (18), followed by calculation of wall shear stress using Equations (2) and (4).

$$C_f = 0.073 * Re_h^{-0.25} \quad (2)$$

$$Re_h = \frac{h * v * \rho}{\mu} \quad (3)$$

$$\tau = \frac{f * \rho * v^2}{2} \quad (4)$$

Where:

τ is the wall shear stress at the wall (Pa),

v is the fluid velocity in the TCFC (m/sec)

C_f is the Dean's friction factor of the channel

ρ is the density of the fluid (kg/m³), which is a function of temperature

μ is the viscosity of the fluid (kg/m.s), which is a function of temperature

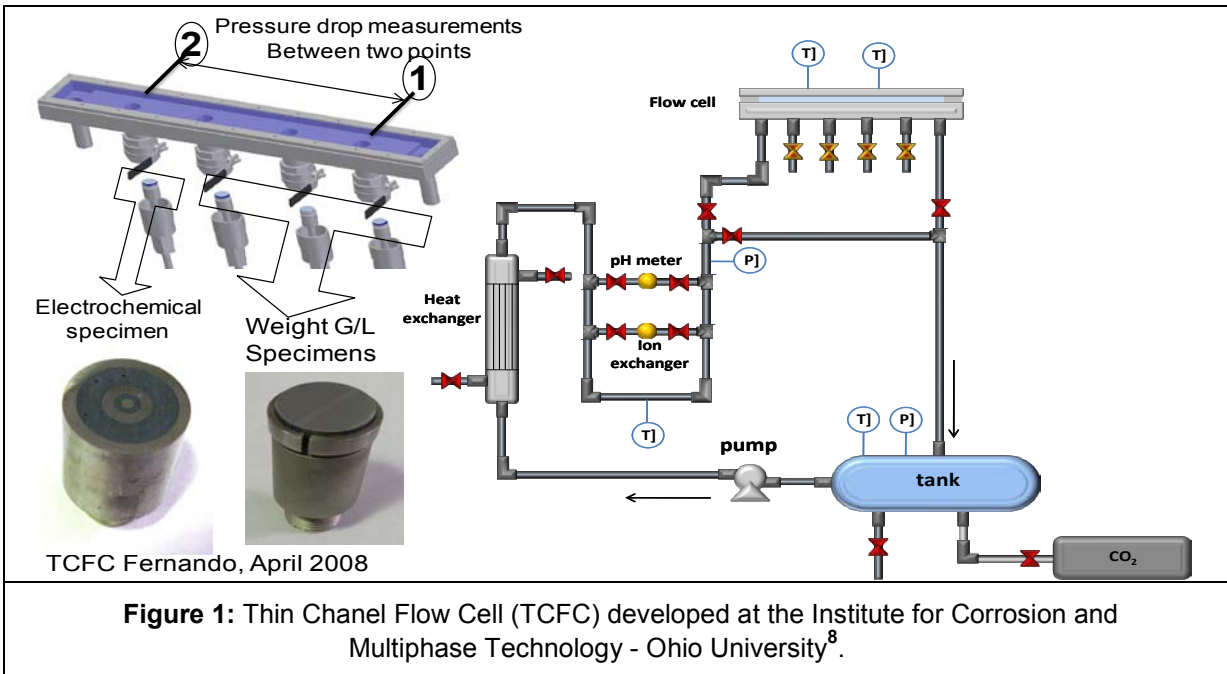
p_1 is the measured upstream pressure (Pa)

p_2 is the measured downstream pressure (Pa)

h is the height of TCFC channel (m),

w is the width of TCFC channel (m)

l is the length between p_1 and p_2 in the TCFC (m), Re_h is Reynolds number.



[§] "Wall shear stress Sensors/Inline Viscometers". 105 Lock St. Suite 301 – Newark, NJ 07103, <http://www.lenterra.com/products/shear-stress-sensors/>. 2012

Effect of Flow on Formed Iron Carbonate Corrosion Product Layer

Specimen Material

- Ten cylindrical specimens (1.25”D, flat weight loss specimens) machined from each steel, with specific dimensions to fit the corrosion specimen holders that were used in TCFC experiments. In each experiment, one specimen was used for weight loss and the other preserved for surface analysis.
- Linear polarization resistance (LPR) probes were custom designed and built consisting of a concentric ring working electrode (WE) made from the same steel being tested and a center pin reference electrode (RE) made from 306 stainless steel.

Electrolyte

An aqueous electrolyte was prepared from deionized water with 1wt. % NaCl. The solution was initially deoxygenated by bubbling with CO₂. This procedure assured that the dissolved oxygen levels were kept well below 20 ppb. The pH of the solution was adjusted by adding deoxygenated acid (HCl) or base (NaHCO₃) in sufficient quantity to reach the desired pH.

Procedure

An iron carbonate layer was generated on each steel by adjusting the concentration of Fe²⁺ ions, temperature, and pH to the desired levels as shown in Table 2. During the protective layer formation experiments, the volumetric flow from the pump was minimized for a flow velocity through the TCFC of 3.5 m/s (30 Pa wall shear stress) and kept constant for 2 days. These steps ensured surface coverage by the protective iron carbonate layer, as judged by the corrosion rate, which was followed by the LPR measurements. When the protective layer formation was judged complete, the flow rate was increased and the specimens were exposed to high wall shear stress (535 Pa) for 3 days.

For the LPR technique, the working electrode was polarized ± 10 mV vs. E_{corr} . After exposure, the specimens were removed and rinsed immediately in isopropyl alcohol and then dried with cool air and stored in a desiccator, which contains an appropriate flow of nitrogen to facilitate full dessication, until analysis by scanning electron microscopy (SEM) was conducted. After analysis of the corrosion product layer, the weight loss specimens were de-scaled using Clarke solution procedure¹⁰ and corrosion rates were determined from the weight loss. Then visual and infinite focus microscopy (IFM) observations were conducted to qualify the steel surface for any possible localized corrosion.

Table 2
Test Matrix: TCFC experiments (Localized Corrosion)

Parameters	Generate iron carbonate layer	Remove iron carbonate layer
Test time	2 days	3 days
Velocity	3.5 m/s	16m/s
wall shear stress	30 Pa	535 Pa
Temperature	80° C	
Total Pressure	2.0 bar	
CO ₂ Partial pressure	1.5 bar	
pH	6.6 (HCl, NaHCO ₃)	
Solution	1.0 wt.% NaCl	
Material	X52, X65 I, X65 II, X70, A106 GRB	
Measurement methods	LPR & weight loss	
surface morphology	IFM, SEM	
Initial [Fe ⁺⁺] concentration	18-22 ppm	

RESULTS AND DISCUSSION

Metallographic Analysis

The micrograph images were examined to determine the microstructure of these steels by comparing the obtained images with a collection of materials micrographs, which have been provided by Micrograph Library, University of Cambridge¹¹.

The microstructures of these steels are described below:

X65I & X70: These steels are quenched & tempered (Q & T) and the microstructure consists of tempered martensite, as shown in Figure 2. The microstructures of X65I and X70 are slightly different; the difference could be due to the different carbon content.

X65 II: This steel is normalized hot rolled and contains a very low amount of carbon (0.07C) so the resulting microstructure of this steel is ferrite with small amount of pearlite. As shown in Figure 3, there is significant difference in microstructure between planes B, C and plane A. As shown in Figure 3-a, the microstructure of plane A consists of thick light bands of ferrite and thin dark bands of pearlite, which indicate that the steel was probably hot rolled, followed by air cooling to room temperature. Some of the pearlite bands contain yellow gains, which could be related to Cu or Mn. As shown in Figure 3-b, the microstructure of planes B and C consists of light grains of ferrite with some dark pearlite.

X52& A106GRB: These steels are normalized and the microstructure consists of large dark grains of pearlite surrounded by large light grains of ferrite, as shown in Figure 4.

Clearly different steel microstructures are seen. A summary of chosen steel microstructure and heat treatment is shown in Table 3. There are two steels with large amounts of pearlite, one ferritic steel with only a bit of pearlite and two Q&T steels. This broad variety of microstructures

may influence the development of iron carbonate precipitation on the surface and the nature of the corrosion product that develops. The goal of this work was to challenge these protective layers to see if they will fail and lead to localized corrosion.

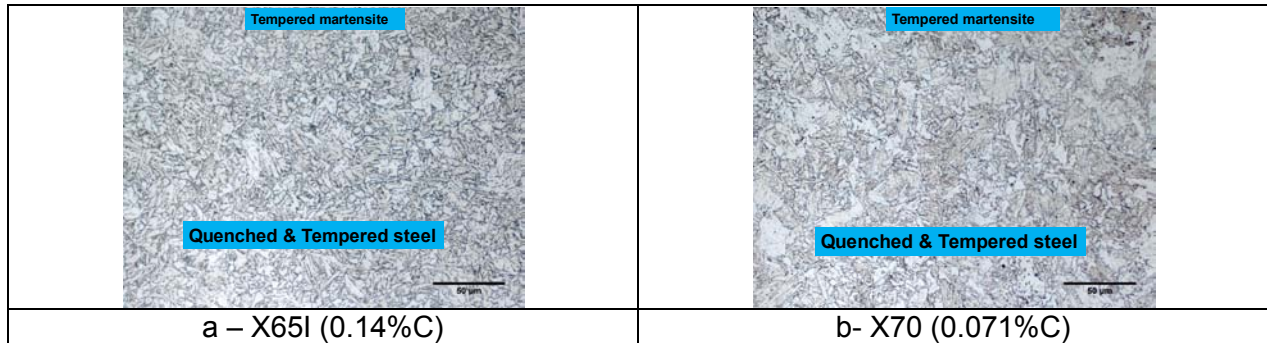


Figure 2: Q&T Steels (X65I and X70) microstructure consists of tempered martensite.

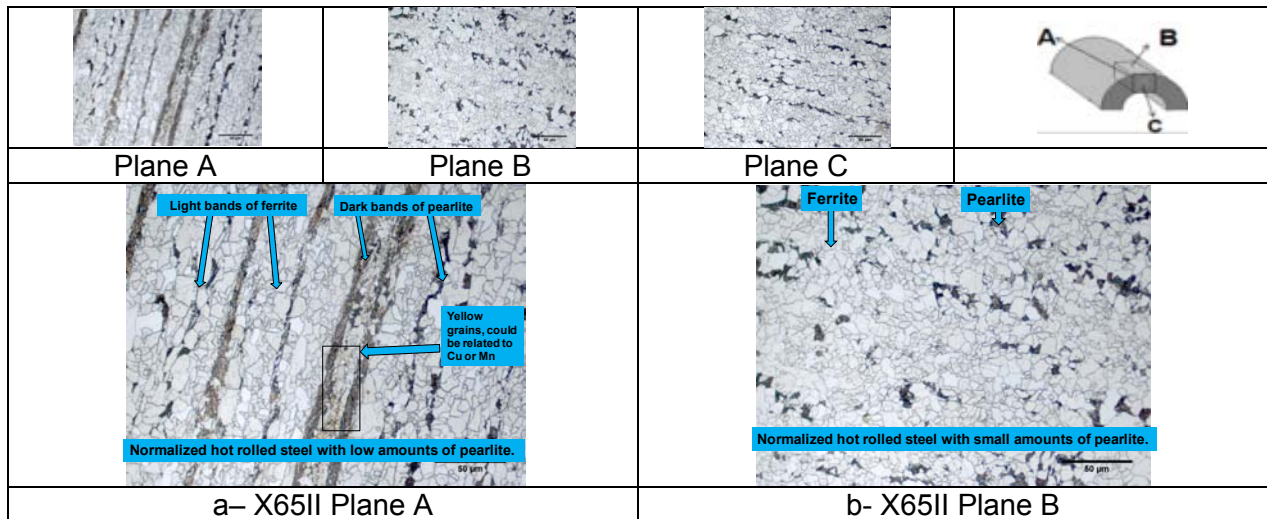


Figure 3: Microstructure of X65II, a normalized hot rolled steel.

a- microstructure consists of thick bright bands of ferrite and thin dark bands of pearlite.
 b- microstructure consists of small bright ferrite with low amounts of pearlite.



Figure 4: Normalized Steels (X52 and A106BRB) microstructure consists of large dark pearlite surrounded by large bright ferrite.

Table 3

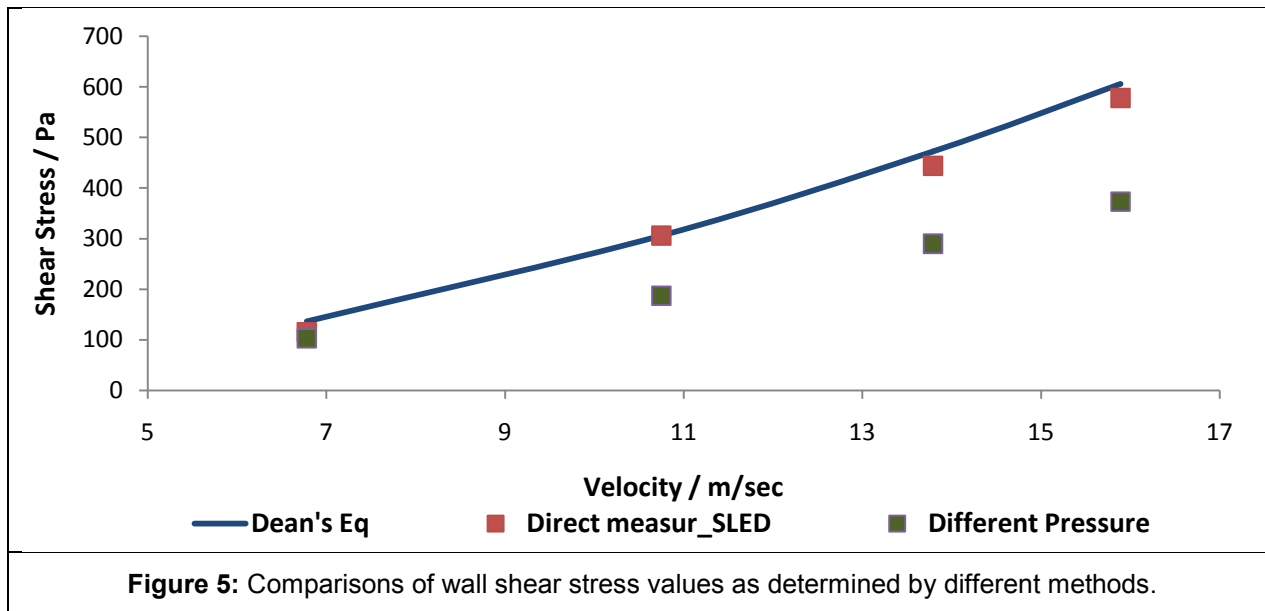
Microstructure and heat treatment of chosen steels.

Steel	Carbon content wt%	Microstructure	Heat treatment
X65I	0.14	Tempered Martensite	Quenched & Tempered
X70	0.071		
X65II	0.07	Ferrite with small amount of pearlite	Normalized hot rolled
X52	0.27	Large dark grains of pearlite surrounding by large light grains of ferrite	Normalized
A106GR B	0.26		

Corrosion Experiments

Wall shear stress Determination

Figure 5 shows the comparisons between the three methods that have been used to determine the wall shear stress. From the graph it is clear that data collected by direct measurement agree with calculations using Dean's formula for wall shear stress. The maximum wall shear stress generated in the TCFC was 535 Pascal.



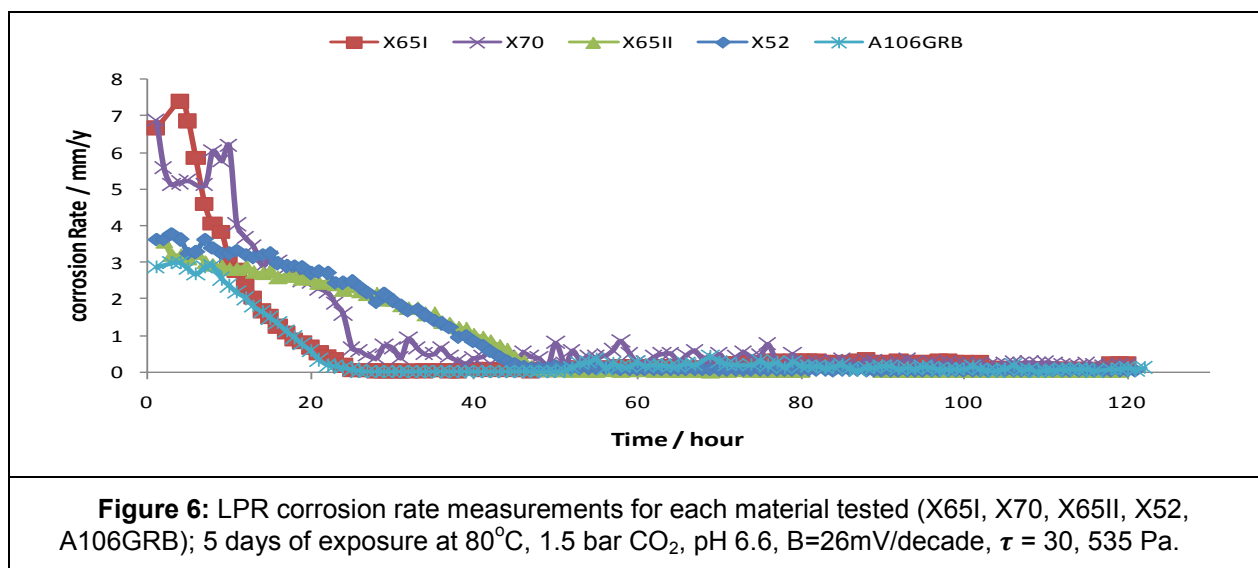
Iron carbonate Layer Formation and Removal Experiments

Variation of the LPR corrosion rate of all steels with exposure time is shown in Figure 6. No increase in the general corrosion rate, as measured by LPR, was noted beyond 2 days. This indicates that the steels surface was covered by a protective iron carbonate layer.

For all steels, after 2 days, the first specimen was removed from the TCFC to document the developed iron carbonate layer and the wall shear stress was then increased to 535 Pa for the

remainder of the experiment. After 5 days of exposure, the two remaining specimens were removed for weight loss corrosion rate measurements and surface analysis.

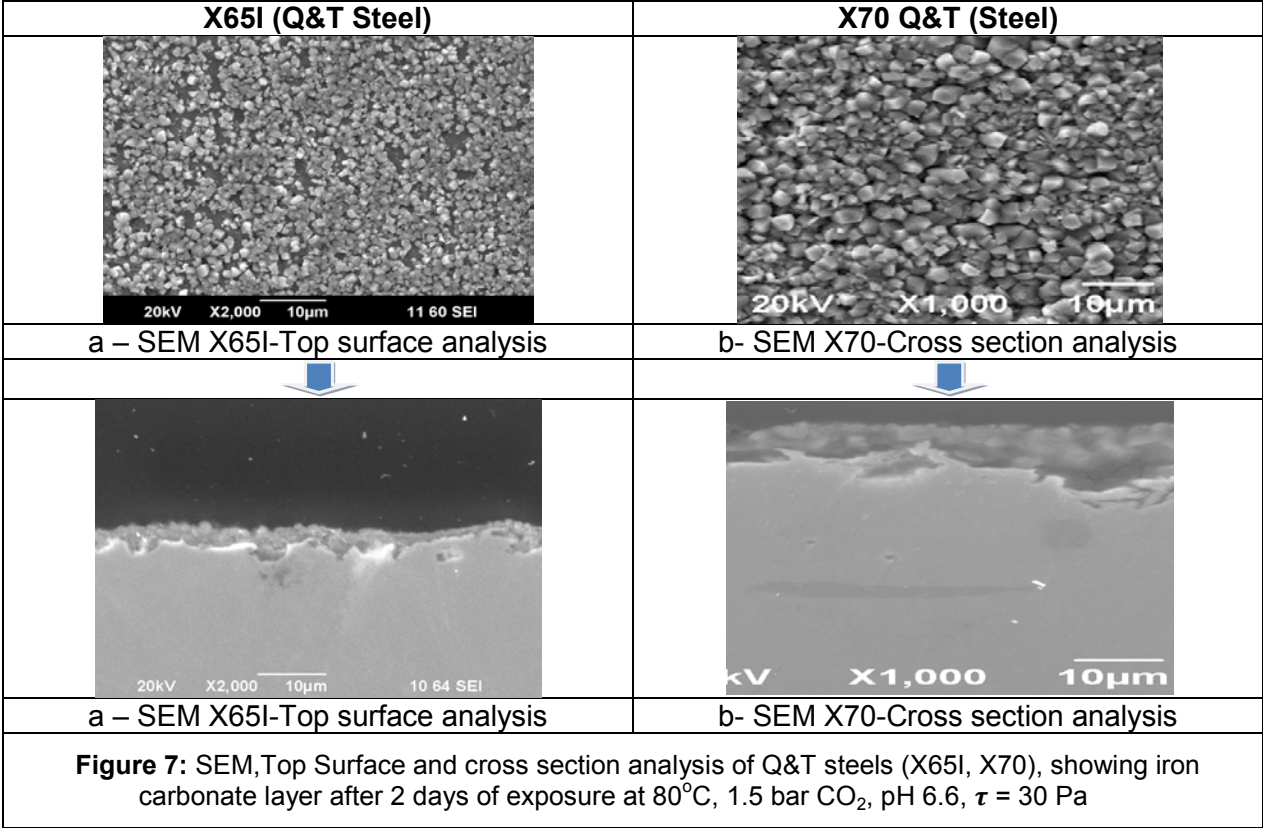
X65I steel: The top surface and cross section analysis of the corroded steel surface by SEM exposed for 2 days at lower wall shear stress show that the specimen was mostly covered with iron carbonate layer see Figure 7-a. After 5 days of exposure the time and space averaged corrosion rate measured by weight loss was found to be 2.1 mm/y, Figure 12-a, what was almost twice as much as was obtained from the integration of the LPR data. This suggests that probably the B value used here was underestimated.

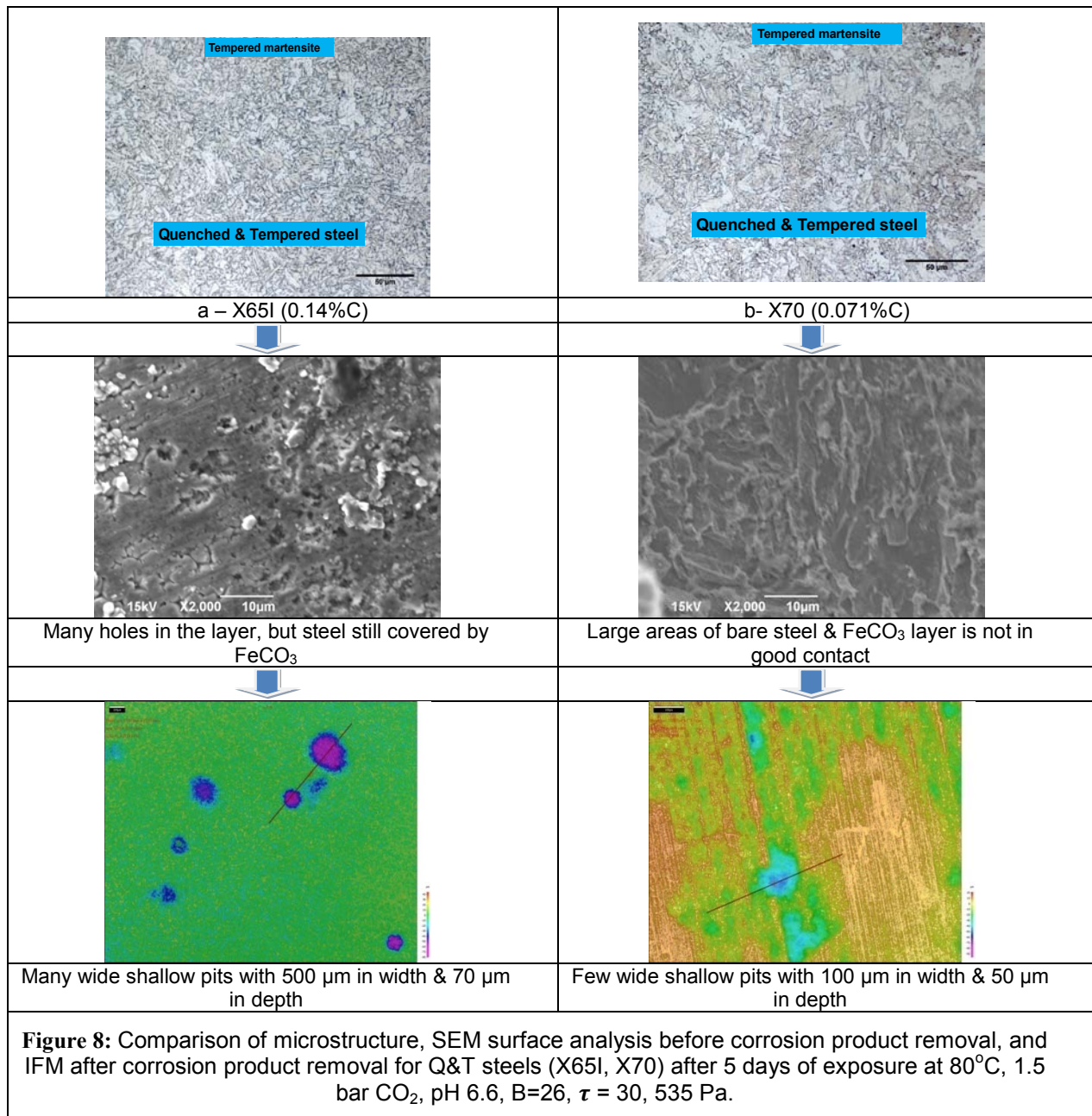


The images that were taken by SEM upon removal of the specimens from the system after 5 days of exposure show that the iron carbonate crystals are removed from some areas after the wall shear stress increase, Figure 8-a, contains. In addition to the top surface analysis, the IFM analysis of the specimen after removing the corrosion product layer shows many wide pits of different sizes. Figure 8-a shows two pits with about 70 μm in depth and about 500 μm in width. The calculated time averaged pit penetration rate was high (about 5 mm/y) which was of the same order of magnitude as the bare steel corrosion rate. Figure 12-b shows comparison between the weight loss corrosion rate and maximum penetration rate for this and other steels.

X70 steel: The top surface and cross section analysis by SEM upon removal of the specimens from the system after 2 days of exposure show that the specimen was mostly covered with the iron carbonate layer, Figure 7-b. After 5 days of exposure, the two remaining specimens were removed and the corrosion rate measured by weight loss was found to be 4 mm/y, Figure 12-a.

The images that were taken by SEM after 5 days of exposure show that the specimen was not fully covered with an iron carbonate layer, there are large areas where the layer was removed by flow, as shown in Figure 8-b. Additionally, the IFM analysis of the specimen surface after removing the corrosion product layer shows some pits of different sizes. Figure 8-b shows a pit with 50 μm in depth and about 200 μm in width. The pit penetration rate was calculated to be 3.5 mm/y which is in the same range as the bare steel corrosion rate. Figure 12-b shows comparison between the weight loss corrosion rate and maximum pit penetration rate for this steel.





X65II steel: The top surface and cross section analysis of steel by SEM upon removal of the specimens from the system after 2 days of exposure show that the specimen was fully covered with iron carbonate layer see Figure 9-a After 5 days of exposure, the two remaining specimens were removed and the time and space averaged corrosion rate measured by weight loss was found to be 1.25 mm/y, Figure 12-a.

The images that were taken by SEM upon removal of the specimens from the system after 5 days of exposure show that the specimen remained mostly covered by an iron carbonate layer, as shown in Figure 10-a. However, the comparison of SEM images before and after the

increase in wall shear stress shows that the iron carbonate layer after wall shear stress increase, Figure 10-a, contains more voids or holes compared with the specimen before the wall shear stress increase, Figure 9-a. The IFM analysis of the specimen after removing the corrosion product layer from the steel specimen shows several pits with different sizes. Figure 10-a, shows a pit with 80 μm in depth or a 5.8 mm/y pit penetration rate which is of the same order of magnitude as the bare steel corrosion rate. Figure 12-b shows comparison between the corrosion rate and penetration rate of the deepest pit.

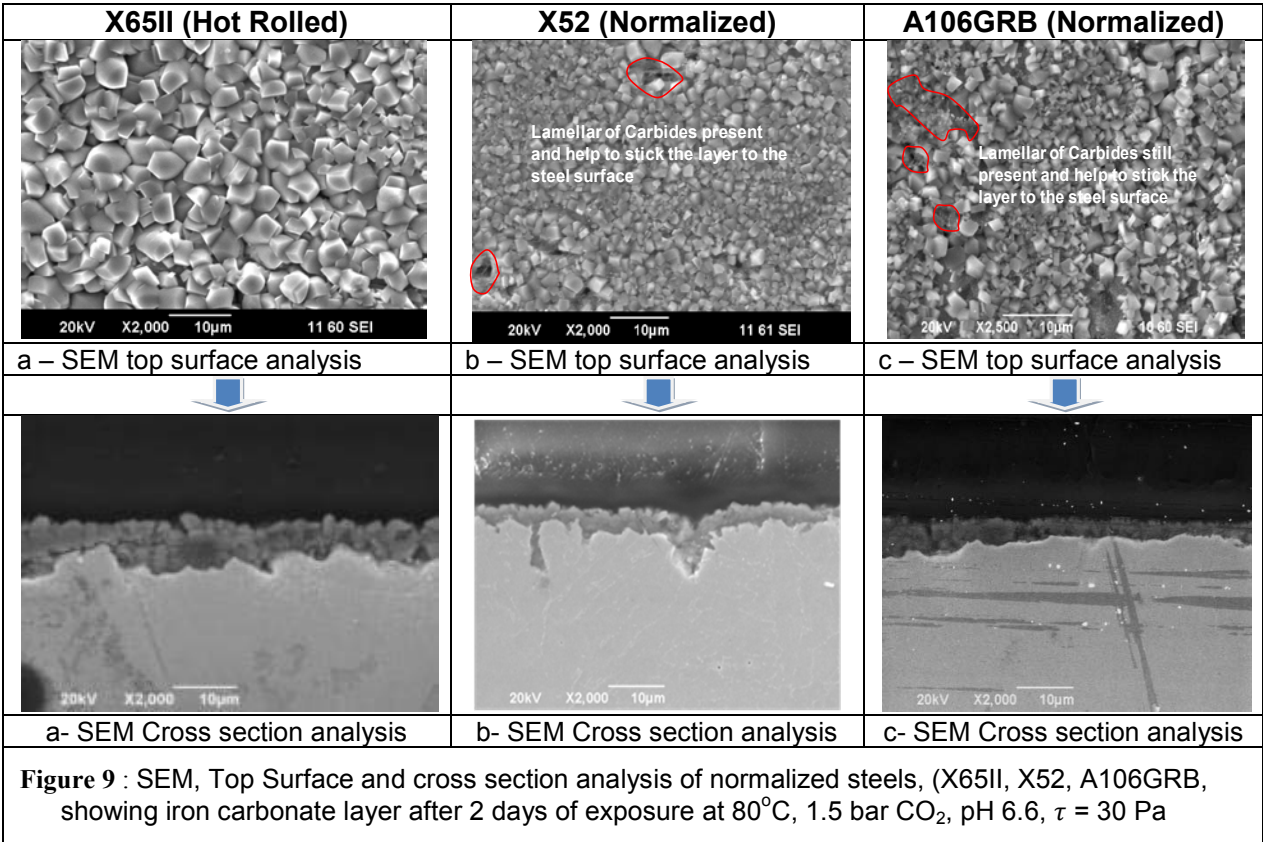
X52 steel: The top surface and cross section analysis of steel by SEM upon removal of the specimens from the system after 2 days of exposure show that the specimen was fully covered with iron carbonate layer see Figure 9-b. After 5 days of exposure, the two remaining specimens were removed and the time and space averaged corrosion rate measured by weight loss was found to be 0.75 mm/y, Figure 12-a.

The images that were taken by SEM upon removal of the specimens from the system after 5 days of exposure show that the specimen remained mostly covered by an iron carbonate layer, as shown in Figure 10-b. The IFM analysis of the specimen after removing the corrosion product layer from the specimen surface shows some pits of different sizes. Figure 10-b shows a pit with 12 μm in depth and about 400 μm in width. The pit penetration rate was 0.8 mm/y. Figure 12-b, shows comparison between the corrosion rate and penetration rate of the deepest pit.

A106GRB steel: The top surface and cross section analysis by SEM upon removal of the specimens from the system after 2 days of exposure show that the specimen was fully covered with an iron carbonate layer, Figure 9-c. In addition to the top surface and cross-section analysis, the cross-section specimen was etched with 2% Nital and analyzed using SEM to see the relationship between the microstructure of steel and the iron carbonate layer. Figure 11 shows strips or lines of iron carbides extending from the steel substrate into the iron carbonate layer at pearlite grains. This iron carbide structure is thought to enhance the adhesion of the layer in the pearlite areas.

After 5 days of exposure, the two remaining specimens were removed and the time and space averaged corrosion rate measured by weight loss was found to be 0.75 mm/y, Figure 12-a.

The images that were taken by SEM upon removal of the specimens from the system after 5 days of exposure show that the specimen appears to be fully covered with an iron carbonate layer, Figure 10-c. Additionally, the IFM analysis of the specimen after de-scaling the specimen shows small pits of different sizes. Figure 10-c shows a pit with 32 μm in depth or 2.3 mm/y pit penetration rate. Figure 12-b, shows comparison between the corrosion rate and penetration rate of the deepest pit.



©2013 by NACE International.
 Requests for permission to publish this manuscript in any form, in part or in whole, must be in writing to NACE International, Publications Division, 1440 South Creek Drive, Houston, Texas 77084.
 The material presented and the views expressed in this paper are solely those of the author(s) and are not necessarily endorsed by the Association.

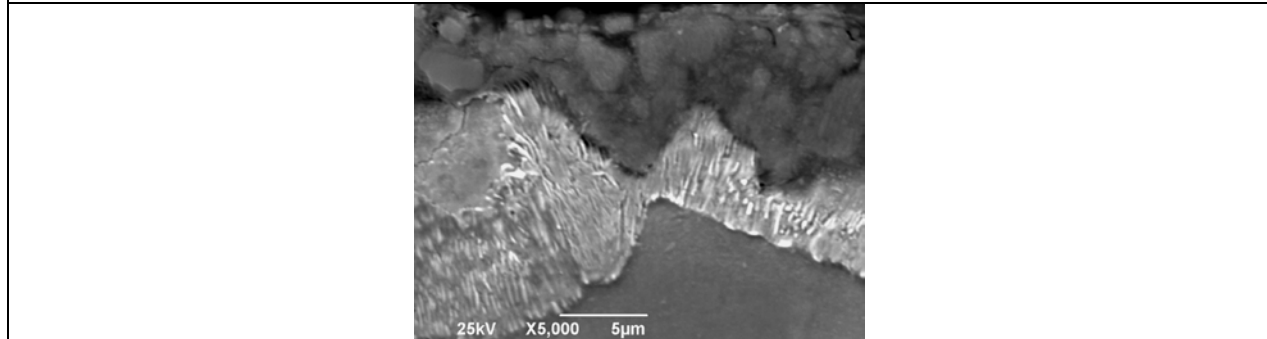
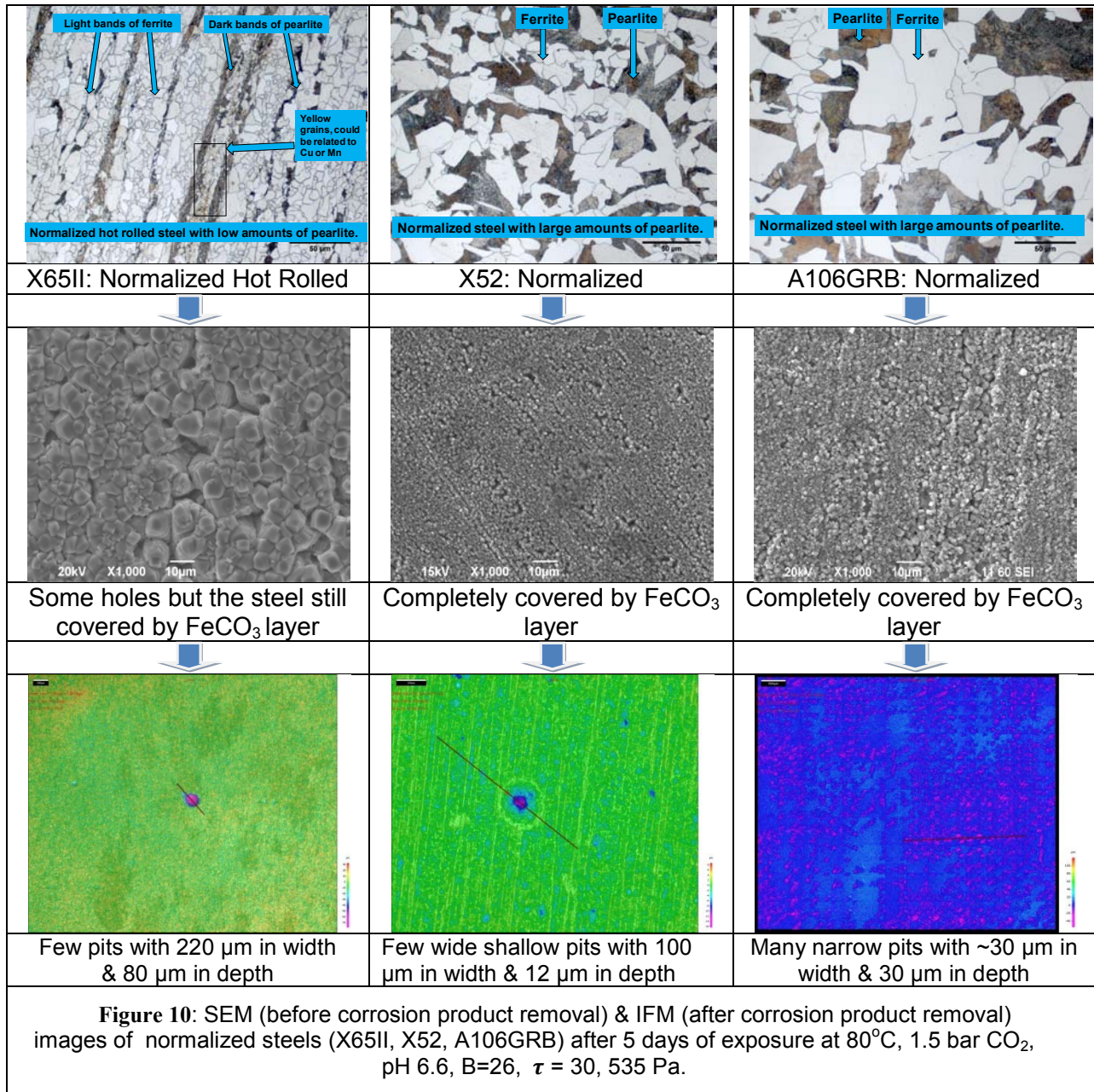


Figure 11: Etched cross section sample of A106GRB steel showing detail of iron carbonate layer & microstructure after 2 days of exposure at 80°C, 1.5 bar CO₂, pH 6.6, τ = 30 Pa.

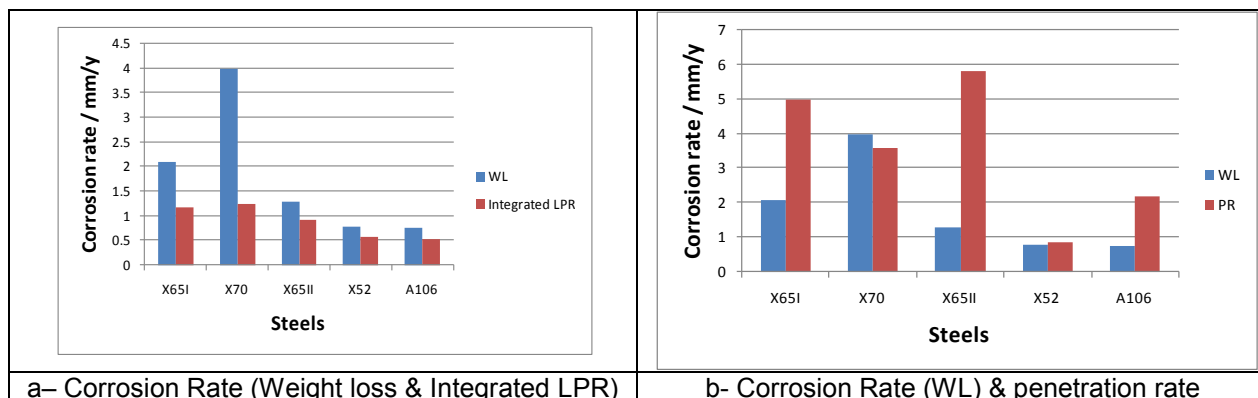


Figure 12:

- a- TCFC corrosion rate measured by weight loss (W/L) & integrated LPR after 5 days of exposure at 80°C, 1.5 bar CO₂, pH 6.6, $\tau = 30$, 535 Pa.
- b- Comparison between corrosion rates measured by weight loss (W/L) & penetration rate of the deepest pit on each steel (P/R) LPR after 5 days of exposure at 80°C, 1.5 bar CO₂, pH 6.6, $\tau = 30$, 535 Pa.

CONCLUSION

- Increasing the wall shear stress caused some locations of the iron carbonate corrosion product layer to fail which may have lead to a high rate of attack (of the same order of magnitude as bare steel corrosion).
- The iron carbonate removal and the pit penetration rates in normalized steels (X52 & A106GRB) were much lower than that of Q & T steels (X65I & X70).
- The low penetration rates in normalized steels can be related to the homogeneity of microstructure and the pearlite structures which help the iron carbonate layer stay attached to the steel surface.
- The hot rolled steel X65II had the largest pitting penetration rates that could probably be due to inclusions.

ACKNOWLEDGMENT

The author would like to thank the *Ministry of Higher Education – Libya* for financial support, S. Smith (Adjunct Professor for Ohio University, ICMT) and Chevron Corp for technical support. Also thank to all member companies that provide support to the corrosion center.

REFERENCES

1. D.A. Lopez, T. Perez, and S.N. Simison, "The influence of microstructure and chemical composition of carbon and low alloy steels in CO₂ corrosion. A State-of-the-art appraisal" *Elsevier Ltd, Material & Design*, vol. 24, pp. 561-575, 2003.
2. A. Dugstad, H. Hemmer, and M. Seiersten, "Effect of Steel Microstructure upon Corrosion Rate and Protective Iron Carbonates Layer Formation," *Corrosion/2000*, Houston, TX, NACE, Paper. 24.
3. J. Crolet, N. Thevenot, and S. Nestic, "The role of conductive corrosion products in the protectiveness of corrosion layers," *Corrosion*, Vol. 54, no 3, pp.194 –203, 1998.
4. D. Clover, B. Kinsella, B. Pejicic, and R. De Marco, "The influence of microstructure on the corrosion rate of various mild steels ," *Applied Electrochemistry*, vol. 35, no 2, pp. 139-149, 2005.
5. T. Berntsen, M. Seiersten, and T. Hemmingsen, "Effect of FeCO₃ supersaturation and carbide exposure on the CO₂ corrosion rate of mild steel," *Corrosion/2011*, Houston, TX, NACE, Paper. 11072.
6. E. Gulbrandsen, R. Nyborg, T. Loland, and K. Nisancioglu, "Effect of steel microstructure and composition on inhibition of CO₂ corrosion," *Corrosion/2000*, Houston, TX, NACE, Paper. 23.
7. Chevron Corporation, Energy Technology Company, FE - MEE - Corrosion Lab 3901 Briarpark Dr., WP117, Houston, TX 77042 U.S.A.
8. Institute for Corrosion and Multiphase Technology, Ohio University, Research Park, 342 West State Street, Athens, Ohio 45701, Tel: 740-593-0283, Fax: 740-593-9949
9. R. B. Dean. "Reynolds Number Dependence of Skin friction and other Bulk Flow Variables in Two-dimensional Rectangular Duct Flow," *J. Fluids Eng*, vol. 100, no 2, pp. 219-242, 1978.
10. ASTM Standard G1, 2003, "Standard Practice for Preparing, Cleaning, and Evaluating Corrosion Test Specimens," ASTM International, West Conshohocken, PA, 2003, DOI: 10.1520/G0001-03, www.astm.org.
11. Micrograph Library, 2004, University of Cambridge. Available: www.doitpoms.ac.uk/miclib/index.php.